



Characterization of Cellulose Nanocrystals Extracted from Sugarcane Bagasse for Potential Biomedical Materials

Nga Tien Lam¹ · Rungsima Chollakup² · Wirasak Smitthipong³ · Thidarat Nimchua⁴ · Prakrit Sukyai¹

Received: 7 October 2016 / Accepted: 26 December 2016 / Published online: 7 January 2017
© Society for Sugar Research & Promotion 2017

Abstract Cellulose nanocrystals (CNCs) were extracted by sulfuric acid from cellulose purified via an environmentally friendly method. In this study, cellulose obtained from sugarcane bagasse (SCB) using steam-exploded and enzyme-treated pretreatment was confirmed using chemical composition analysis to have a 92.59 ± 0.12 whiteness index and 87% α -cellulose content. The morphology of extracted CNCs, characterized using atomic force microscopy images, transmission electron microscopy images and energy-dispersive x-rays, showed the diameter and length were in the ranges 9.8 ± 6.3 and 280.1 ± 73.3 nm, respectively, with an expected ratio (L/d) of 20–25 and a low concentration of sulfate (0.2%) on surface particles. Moreover, fourier transformed infrared spectroscopy and X-ray diffraction results demonstrated free noncellulosic contents and an improved crystallinity for CNCs, respec-

tively. A decrease in the thermal stability of CNCs was examined by thermogravimetric analysis, and no evidence of cytotoxicity in the CNCs was obtained. The isolated CNCs from SCB may be considered as a potential biomedical material.

Keywords Cellulose nanocrystals · Cytotoxicity · Sugarcane bagasse · Xylanase

Introduction

In the last few decades, there has been a trend to utilize biodegradable and renewable material which is sourced from agricultural residues such as coconut husks (Rosa et al. 2010) and sugarcane bagasse (Teixeira et al. 2011). Sugarcane bagasse is the residual fraction of sugarcane after juice extraction in the sugar production process (Bhattacharya et al. 2008). Similar to other lignocellulose components, SCB is consisted of a complex network of carbohydrate polymers including lignin, hemicellulose, cellulose and pectin (Sun et al. 2004). A great deal of previous literature indicated that nearly one-half (40–50%) of the raw material weight from SCB is cellulose (Bhattacharya et al. 2008). Due to the high concentration of cellulose, SCB becomes a potential source for cellulose extraction to be used in recyclable materials. In recent decades, SCB has been well known for its three main components: (1) lignin, which is formed from complex aromatic rings (Zuluaga et al. 2009); (2) hemicellulose, an amorphous polymer with rich lateral chains consisting of diverse sugars; and (3) cellulose identified by a linear homopolymer made from anhydroglucose units linked by β -glycosidic bonds (Gilbert and Kadla 2000). Generally, the disruption of the natural matrices of the lignin,

✉ Prakrit Sukyai
fagipks@ku.ac.th

¹ Biotechnology of Biopolymer and Bioactive Compounds Laboratory, Department of Biotechnology, Faculty of Agro-Industry, Kasetsart University, Chatuchak, Bangkok 10900, Thailand

² Kasetsart Agricultural and Agro-Industrial Product Improvement Institute (KAPI), Kasetsart University, Chatuchak, Bangkok 10900, Thailand

³ Department of Materials Science, Faculty of Science, Kasetsart University, Chatujak, Bangkok, Thailand

⁴ Enzyme Technology Laboratory, Bioresources Technology Unit, National Center for Genetic Engineering and Biotechnology (BIOTEC), 113 Thailand Science Park, Phahonyothin Road, Khlong Nueng, Khlong Luang, Pathum Thani 12120, Thailand

hemicellulose, cellulose and others components has been carried out during using chemical agents and physical force (Brinchi et al. 2013). Thermal pretreatment with steam-exploded force has been used in many studies as it is not only acts as a defibrillating agent but also decomposes the macro-polymers into low molecular weight fractions (Zheng et al. 2014). An environmentally friendly process with xylanase assistance to diminish the need for bleaching chemicals can be employed effectively after explosion pretreatment (Saelee et al. 2016). This helps to partially dissolve the hemicellulose content and is followed by sodium chloride to totally destroy noncellulosic matter (Zuluaga et al. 2009; Mandal and Chakrabarty 2011).

Cellulose in nano-sized particles—known as nanocellulose (NC)—is a promising potential biomaterial, having a nanoscale dimension, high specific strength and modulus, high surface area and unique optical properties (Dri et al. 2013; Wu et al. 2012). A detailed study of cellulose fiber structure indicates that cellulose possesses high compact domains, crystal areas, is stabilized via hydrogen bonding and is disrupted by disordered fractions and amorphous regions. Thus, cellulose nanocrystals (CNCs) extraction is the elimination of amorphous fractions in cellulose fiber by acid hydrolysis such as by using sulfuric acid (H_2SO_4) (Mandal and Chakrabarty 2011) or hydrochloric acid (HCl) (Teixeira et al. 2011). Typically, CNCs are rigid, rod-like crystals with a diameter in the range 10–20 nm and a length of 100 nm (Mandal and Chakrabarty 2011; Teixeira et al. 2011). The main features that stimulate the use of CNCs as polymer reinforcement agents are its large specific surface area, very high modulus of elasticity (approximately 150 GPa), biocompatibility and biodegradability (Šturcová et al. 2005; Mariano et al. 2014; Petersson and Oksman 2006). In the mammalian body, cellulose exhibits a relative low protein adsorption and cell adhesion and a low immune response. Moreover, nanocellulose can provide a cell-friendly environment to encourage cell attachment and proliferation as a special tissue bio-scaffold. No significant cytotoxicity to various human cell lines was found in previous studies (Zhou et al. 2013; Male et al. 2012).

There is no earlier report work on evaluating toxicity for the cell line of CNCs extracted from SCB. Moreover, this study applied the process with xylanase-assisted pretreatment for cellulose purification that has been recorded in bleached agent reduction and also not discussed in any previous literature for cellulose preparation to extract CNCs. Thus, the objective of this study was to isolate cellulose nanocrystals (CNCs) from extracted cellulose via an environmentally friendly process and to characterize the CNCs obtained in terms of their morphology, crystallinity, thermal behavior and cytotoxicity for biomedical application.

Materials and Methods

Sugarcane bagasse was obtained from the Kaset Thai International Sugar Corporation Public Company Limited factory, Nakhonsawan, Thailand. Xylanase ($1568.57 \pm 2.31 \text{ U mL}^{-1}$) was supplied by The National Center for Genetic Engineering and Biotechnology (BIOTEC), Thailand Science Park, Thailand.

Cellulose Extraction

Bagasse was washed with water to remove artifacts, followed by drying at 55 °C for 24 h. Dried SCB was pretreated using a steam-explosion machine (Nitto Koatsu 2.5 L, Japan) at a pressure of at least 1.3 MPa (190 °C) for 15 min. Then, the steam-exploded bagasse was digested using xylanase, at 20 U g^{-1} (solid–liquid ratio 1:15 (w/v)), under agitation. The experiment was carried out at 50 °C for 2 h (Saelee et al. 2016). Bleached fiber was obtained after treating with 1.4% (w/v) sodium chlorite (NaClO_2) solution at pH 4 which was adjusted by acetic acid at 70 °C for 6 h (Mandal and Chakrabarty 2011). NaClO_2 and acetic acid were added every hour until a white bleached fiber was obtained. The resulting suspension was filtered and washed with distilled water until the pH reached 6–7.

Nanocellulose Preparation

About 5 g of cellulose was dispersed in 100 mL of 60% (w/v) sulfuric acid hydrolysis (solid–liquid ratio 1:20) at 45 °C for 75 min with continuous stirring (500 rpm). The hydrolysis was quenched by adding 500 mL water to the reaction mixture, and then the slurry was washed with distilled water for 15 min at 15,000 rpm, using repeated centrifugation. The supernatant was removed from the sediment and replaced by clean distilled water and mixed; the centrifugation step continued until the pH of the supernatant was 1. The last wash was conducted using dialysis with distilled water until the wash water maintained a constant pH of 7. Then, sonication (Elmasonic Model S100H, Germany) was conducted in an ice bath for 15 min. The aqueous suspension was stored at 4 °C in a fridge for further experiments (Zhou 2012; Kumar et al. 2014).

Color Reflectance Properties

The color values of fibers were measured using a colorimeter (UltraScan XE, Hunter Associates Laboratory, Reston, VA, USA). A white standard plate was used to calibrate the instrument with the color values of $L = 100$, $a = 0$ and $b = 0$. The color of specimens was determined

using an “*L*” value range from 0 (black) to 100 (white), an “*a*” value range from –80 (greenness) to 100 (redness) and a “*b*” value range from –80 (blueness) to 70 (yellowness). The total color difference (ΔE) and whiteness index (WI) were calculated using the equations below (Rhim et al. 1999)

$$\Delta E = (\Delta L^2 + \Delta a^2 + \Delta b^2)^{0.5}$$

$$WI = 100 - \left[(100 - L)^2 + a^2 + b^2 \right]^{0.5}$$

where $\Delta L = L_{\text{standard}} - L_{\text{sample}}$; $\Delta a = a_{\text{standard}} - a_{\text{sample}}$; $\Delta b = b_{\text{standard}} - b_{\text{sample}}$. Three measurements were taken on each sample.

Chemical Composition

Chemical composition of samples of untreated, steam-exploded, enzyme-treated and bleached fibers was evaluated following a standard method of Technical Association of Pulp and Paper Industry standard (TAPPI). According to TAPPI, the lignin concentration was determined by T222 om-98, followed by estimation of the holocellulose contents (α -cellulose and hemicellulose) using the acid chlorite method. Afterward, the α -cellulose percentage was determined according to TAPPI T203 om-88, and hemicellulose was determined by subtracting the α -cellulose component from the holocellulose content. An average of three replicates was calculated for each sample.

Scanning Electron Microscopy Each sample was placed on a steel cylinder and sputtered with gold. Surface morphologies were examined using a scanning electron microscope (Hitachi model, Jeol JSM5600LV, Japan) at an accelerating voltage of 15–20 kV. The energy-dispersive X-ray (EDX) diffractor attached with the SEM unit was operated for CNCs elemental analysis.

Atomic Force Microscopy Measurements were taken in tapping mode using an Asylum model MFP-3D AFM (Bio, USA) at ambient temperature. In the sample preparation, a drop of diluted CNCs aqueous suspension of colloid was dispersed on the surface of an optical glass substrate and allowed to dry at ambient temperature and analyzed subsequently.

Transmission Electron Microscopy A CNCs dilute aqueous suspension of 0.01% (w/v) was cast as one drop onto a copper grid with carbon coating followed by negative staining of uranyl acetate of 2% (w/v) for a few minutes. Each sample was dried at room temperature and then observed at 100 keV using TEM analysis (Hitachi model HT7700, Japan).

Fourier Transform Infrared Spectrometer Analysis

Infrared spectra of the samples were recorded using FTIR spectra (Bruker Tensor 27 spectrometer, USA) at room temperature. The sample fractions were dried in an oven at 60 °C for 12 h, mixed with KBr and pressed into pellets. The samples were analyzed over the range 500–4000 cm^{-1} .

X-Ray Diffraction

XRD measurements were taken using an X-ray diffractometer (Philips Analytical X'Pert, the Netherlands) using Cu-K α radiation. The samples were scanned over a range varying over 2θ in the range 10–50°. The crystallinity index (CrI) of cellulose materials was calculated from the height of the 200 peak (I_{200} , $2\theta = 22.6^\circ$) and the intensity minimum between the peaks at 200 and 110 (I_{am} , $2\theta = 18^\circ$) using the Segal method and the equation below (Segal et al. 1962):

$$\text{CrI}\% = \frac{I_{200} - I_{\text{am}}}{I_{200}} \times 100$$

where I_{200} represents both a crystalline and an amorphous material, and I_{am} represents an amorphous material.

Thermogravimetric Analysis

The thermal properties of cellulose fibers were determined using a thermogravimetric analyzer (Mettler Toledo, Model TGA/SDTA 851 $^\circ$, Switzerland) for TGA and derivative thermogravimetric analysis (DTG). The samples were heated from 50 to 600 °C with a scanning rate of 10 °C min^{-1} under a nitrogen atmosphere. The weight of sample was in range 2–5 mg.

Cytotoxicity

Cytotoxicity analysis of the CNCs suspension was performed in accordance with ISO standard 10993-5 that evaluated the cellular response with the test specimen extracts by 3-(4, 5-Dimethylthiazolyl-2)-2, 5-diphenyltetrazolium bromide (MTT) assay. For the indirect cytotoxicity test, mouse fibroblast L929 cells (NCTC clone 929: CCL 1, American Type Culture Collection [ATCC], of Strain *L*) were cultured in minimum essential medium (MEM) at a density of 1×10^5 cells mL^{-1} into a 96-well plate followed by incubation for 24 ± 2 h ($5 \pm 1\%$ CO_2 , 37 ± 1 °C and $95 \pm 5\%$ relative humidity). The CNCs sterilized by ethylene oxide gas (ETO) was placed in 96-well plates and extracted at 37 ± 1 °C for 24 ± 2 h. The number of living cells after incubation was quantified using a 3-(4, 5-Dimethylthiazolyl-2)-2, 5-diphenyltetrazolium bromide (MTT) assay. The viability was calculated as a ratio between the blank and the

sample absorbance that was measured using a microplate reader (Bio-Tek, USA) at 570 nm. The lower the viability value, the higher the cytotoxic potential of the sample (Kirdponpattara et al. 2015; Kuzmenko et al. 2016).

Morphology of Mouse Fibroblast L929 Cell Line

The mouse fibroblast L929 cells (NCTC clone 929; CCL 1, American Type Culture Collection [ATCC], of Strain *L*) were seeded in MEM for 24 h. Then, 0.05 g mL⁻¹ of the CNCs extractive was used to replace the MEM, and a negative control with MEM was incubated for another 24 h at 37 °C. The influence of the CNCs on cells morphology was observed under a trinocular phase contrast microscope (Leica DMIL, Germany).

Result and Discussion

Color Reflectance Properties and Chemical Composition

It is well documented that the high concentration of non-cellulosic components can be attributed to the pigment content of fibers while white fibers have a greater amount of cellulose; thus, the white color of the fiber also indicates the successful removal of noncellulose matter (Teixeira et al. 2010). The whiteness index (WI) was used to estimate values related to the white color which was considered as a measurement of change during the cellulose purification process. The whiteness of untreated fibers was recorded around 63.21 ± 1.33, which was brighter than for the steam-exploded fibers (50.26 ± 1.5) and enzyme-treated fibers (47.31 ± 0.97). Generally, the increased pigment in the steam-exploded fibers resulted from generating lignin that contains chromophore and auxochrome. Hemicellulose is also attributed to various sugar residues and branching chemistry that may be ready to break and release at high temperature in the steam process. The bleaching agent showed its effect on obtaining bleached fiber (with 92.59 WI) after 6 h (Table 1; Fig. 1). The bleaching process may chemically remove colors from materials and leads to a more uniform reflectance. Consequently, increased

delignification usually results in lower color of fibers (Teixeira et al. 2010; Chen et al. 2011).

The chemical composition of the fibers was determined in accordance with the TAPPI standards which were used for α -cellulose (TAPPI T202 om-88) and lignin (TAPPI T222 om-98). Raw fibers recorded a high cellulose concentration (42.46 ± 0.04%) that combined with hemicellulose (33.35 ± 0.48%) and lignin (20.97 ± 0.55%). However, steam-exploded fiber showed a decline in the hemicellulose and lignin contents (14.44 ± 0.28% and 19.58 ± 0.01%, respectively). It is well documented that hemicellulose present on the surface has a weak structure that consists of short lateral chains of different sugars (pentoses, hexoses and acetylated sugars), so that hemicellulose could be easily attacked by diluted acid, alkali or enzymes under mild conditions (Sun et al. 2005). Similarly, hemicellulose was destroyed under the high steam pressure which resulted in the disruption of the lignin and hemicellulose network and lignin degradation to a certain extent (Zhang et al. 2008). Furthermore, due to its branched chains, hemicellulose was continuously degraded by xylanase. Under such circumstances, xylanase catalyzed deacetylated xylan substrates that led to a slightly lower hemicellulose content (12.73 ± 0.22%) of the enzyme-treated fiber than that of steam-exploded fiber (14.44 ± 0.28%) (Roncero et al. 2003). At the end of the purification process, the α -cellulose content (87.4%) of the bleached fiber was twice that of the untreated fiber (42.46%). Moreover, the concentrations of lignin and hemicellulose were substantially decreased after bleaching, with figures of 0.99 and 7.06%, respectively (Table 2). In acidic media, sodium chlorite liberates chlorine that is widely used to increase the removal of lignin including aromatic components (Zuluaga et al. 2009). Bleached fibers were successfully obtained while using an environmentally friendly methodology (Saelee et al. 2016). The decreases in the solid yield of each stage (Table 2) confirmed the removal of noncellulosic components (Kargarzadeh et al. 2012).

Morphology Analysis

The SEM results showed that the morphology of the fiber obtained after each stage had noticeably changed. The untreated fibers contained high concentration of

Table 1 Hunter color values (mean value ± standard deviation) of the L^* , a^* and b^* parameters, the total color difference (E) and whiteness index (WI) functions of the fibers at different stages of treatment

Sample	L^*	a^*	b^*	E^*	WI*
Untreated fiber	66.17 ± 1.42	3.08 ± 0.09	14.13 ± 0.36	30.56 ± 1.29	63.21 ± 1.33
Steam-exploded fiber	52.55 ± 1.56	7.01 ± 0.24	13.15 ± 0.83	43.41 ± 1.49	50.26 ± 1.50
Enzyme-treated fiber	49.75 ± 1.02	7.13 ± 0.19	14.15 ± 0.19	46.35 ± 0.97	47.31 ± 0.97
Bleached fiber	94.79 ± 0.12	0.05 ± 0.01	05.27 ± 0.06	04.54 ± 0.05	92.59 ± 0.12

Fig. 1 Physical appearance of untreated fiber (a), steam-exploded fiber (b), enzyme-treated fiber (c) and bleached fiber (d)

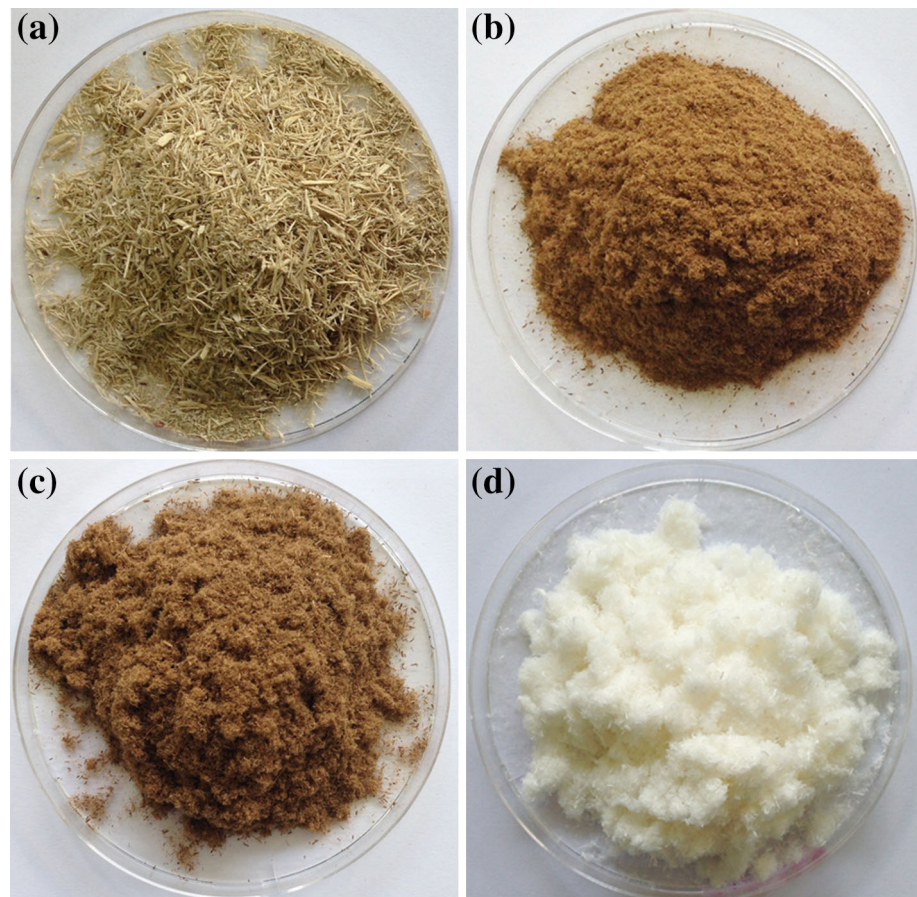


Table 2 Chemical composition (mean value \pm standard deviation) of sugarcane bagasse samples after cellulose purification

Sample	Lignin (%)	Hemicellulose (%)	α -cellulose (%)	Yield (%)
Untreated fiber	20.97 \pm 0.55	33.35 \pm 0.48	42.46 \pm 0.04	100
Steam-exploded fiber	19.58 \pm 0.01	14.44 \pm 0.28	61.37 \pm 0.43	77.40 \pm 3.88
Enzyme-treated fiber	16.60 \pm 0.02	12.73 \pm 0.22	64.53 \pm 0.73	68.32 \pm 0.52
Bleached fiber	0.99 \pm 0.06	7.07 \pm 0.49	87.40 \pm 0.19	50.21 \pm 1.80

extractives (waxes, pectin, oil, etc.) on the fibers surface which contributed to their superficial layers (Fig. 2a) (Mandal and Chakrabarty 2011; Kumar et al. 2012). Steam-exploded fibers had a smaller diameter than that of untreated fibers and presented the elimination of surface impurities along with defibrillation (Fig. 2b). During the steam-explosion stage, the force of the steam acted as an agent to depolymerize and disintegrate the organization of untreated fibers into fiber bundles, opened up the particulate structure of the biomass and further removed amorphous ingredients (lignin, hemicellulose, etc.) (Sun and Cheng 2002; Abraham et al. 2011). This led to a size reduction that enhanced the external surface area of the fibers for enzyme hydrolysis (Marzieh et al. 2015). Clearly, the effect of the enzyme treatment exposed some

damage on the exterior area of fibers such as exfoliation, caving in and fracturing due to the lack of a partial fraction of xylans in the xylanase digestion (Fig. 2c) (Saelee et al. 2016). The bleaching process involving treatment with sodium chlorite in an acid medium resulted in the lignin being eliminated via complex formation and depolymerization. Because of the existence of space on the surface fiber, the bleaching agent readily accessed the interior of the structure. This action led to a diameter decrease in the fibrils to approximately 10–20 μ m, which was smaller than the average size of the fiber bundles (75–150 μ m) before the bleaching treatment. (Figure 2d) (Sun et al. 2004; Mandal and Chakrabarty 2011). Moreover, the bleached fibers were observed as round, fine bundles of fibers with clean, smooth surfaces that

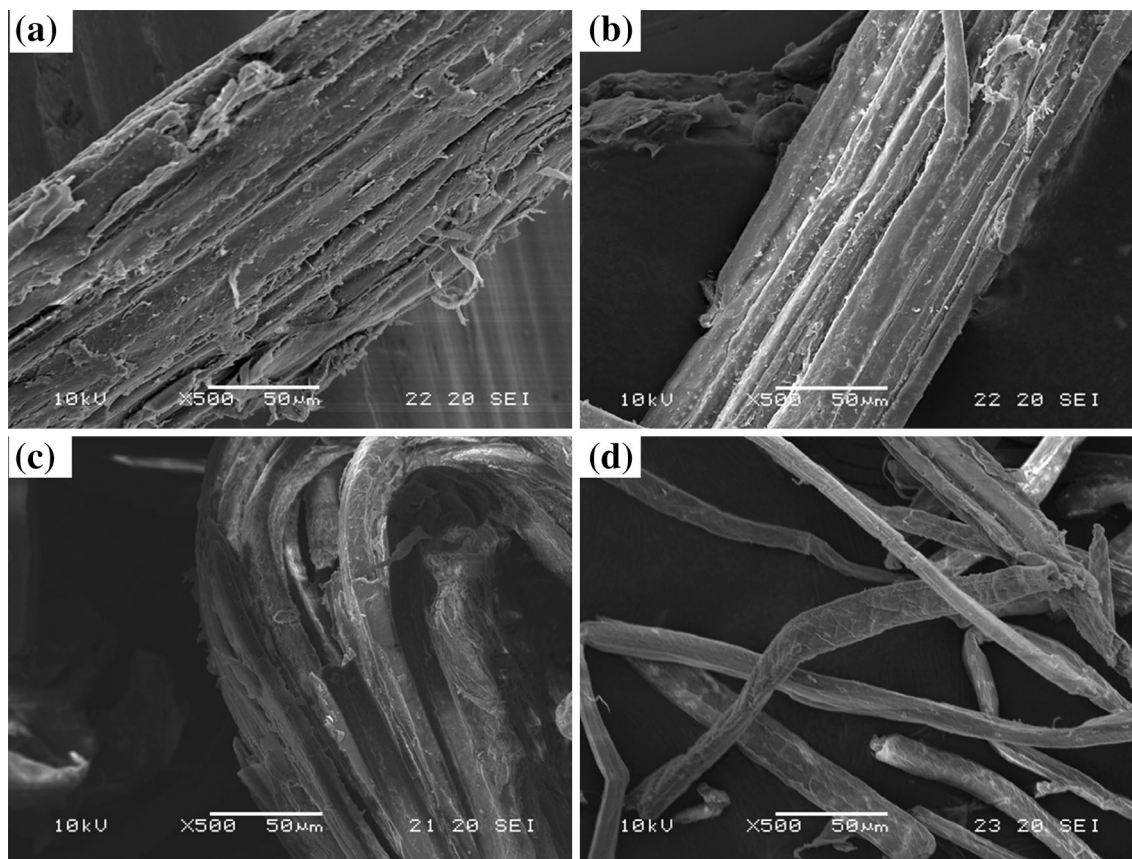


Fig. 2 SEM images of untreated fiber (a), steam-exploded fiber (b), enzyme-treated fiber (c) and bleached fiber (d)

confirmed the removal of wax, pectin, lignin and hemicellulose (Kumar et al. 2012).

Atomic Force Microscopy Analysis, Transmission Electron Microscopy and Energy-Dispersive X-Ray Diffraction

The morphological properties of the CNCs suspension can be observed in Fig. 3a. The CNCs colloid verified the well-suspended state of nanoparticles in distilled water. AFM detected the needle-like morphology of the extracted cellulose at a nanoscale which was similar to the CNCs obtained by Kim and Song (2015). Both the TEM (Fig. 3b) and AFM (Fig. 3c) images display some aggregated nanoparticles and individual nanocrystals perhaps due to the high specific surface area and strong interaction bonds presented among CNCs. From Fig. 3a, b, the CNCs are uniformly dispersed in width and exhibit irregular length. The various dimensions of CNCs can be explained by the differences in raw material sources and extraction conditions (Eichhorn et al. 2010). The average width of CNCs was found to be around 9.8 ± 6.3 nm, and the average length was 280.1 ± 73.3 nm, which resulted in an aspect ratio (*L/d*) of around 20–25 (Fig. 3d).

EDX was used to detect the elemental components in samples to determine sulfuric acid removal by the dialysis process in the CNCs extraction process. Figure 4 shows the EDX spectrum of extracted cellulose nanocrystals and reveals the peaks for carbon, oxygen and sulfur related to their binding energies, respectively. The CNCs spectrum contained 0.2% elemental impurity of sulfur and main components of 52.71% for carbon and 47.09% for oxygen (Table 3). The remaining sulfate groups in the CNCs at a low percentage confirmed that the CNCs colloid was acid-free (Ranby 1949).

Fourier Transform Infrared Spectroscopy

FTIR spectroscopy was carried out to study the chemical functional group changes during the process. Figure 5 shows the FTIR spectra of untreated fiber, steam-exploded fiber, enzyme-treated fiber, bleached fiber and CNCs. The FTIR spectra of all samples exhibited a broad band in the region $3500\text{--}3200$ cm^{-1} that corresponded to the O–H stretching vibration of the OH groups in cellulose molecules (Mandal and Chakrabarty 2011; Elanthikkal et al. 2010). Moreover, the characteristic C–H stretching vibration around 2894 cm^{-1} was found in all samples (Khalil et al. 2001). The peak at 1737 cm^{-1} was associated with

Fig. 3 Physical appearance of cellulose nanocrystals (a), TEM image (b), AFM image (c) and height distribution (d)

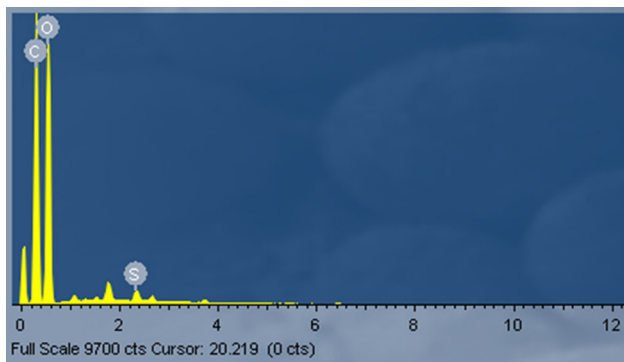
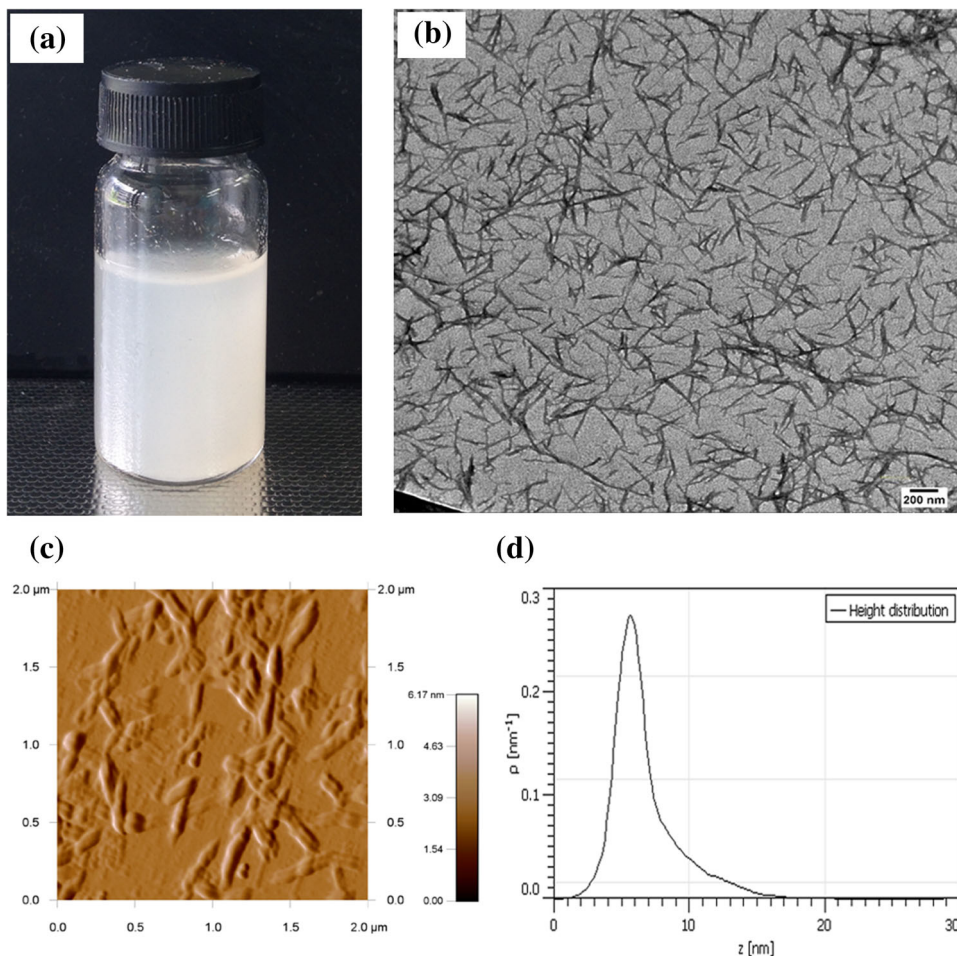


Fig. 4 Energy-dispersive X-ray diffraction result of cellulose nanocrystals

the C=O stretching vibration either of the acetyl and uronic ester groups of the hemicelluloses or of the ester linkage of carboxylic group of the ferulic and *p*-coumaric acids of lignin and/or hemicelluloses (Li et al. 2014; Sun et al. 2005; Elanthikkal et al. 2010). The band at 1632 cm⁻¹ was due to the bending mode of the absorbed water (Sun et al. 2005; Troedec et al. 2008). The peaks at 1514 and

Table 3 Element component (mean value ± standard deviation) of cellulose nanocrystals

Elements	Weight (%)	Atomic (%)
C K	45.45 ± 0.31	52.71
O K	54.05 ± 0.31	47.09
S K	0.47 ± 0.03	0.20
Total	100	

1606 cm⁻¹ were related to the aromatic –C=C– stretch of the aromatic ring present in lignin (Wang et al. 2010). The peak at 1425 cm⁻¹ was due to the –CH₂– bending (Elanthikkal et al. 2010). The vibration peak detected at 1473 and 1365 cm⁻¹ in all samples has been related to the bending vibration of the C–H symmetric and asymmetric deformations, respectively (Sun et al. 2005). The absorbance at 1327 cm⁻¹ is attributed to the C–C and C–O skeletal vibrations (Sun et al. 2005). The peak at 1245 cm⁻¹ presents the C–O out-of-plane stretching vibration of the aryl group in lignin (Troedec et al. 2008). The peak observed in the spectrum at 1054 cm⁻¹ is due to the C–O–C pyranose ring (antisymmetric in phase ring)

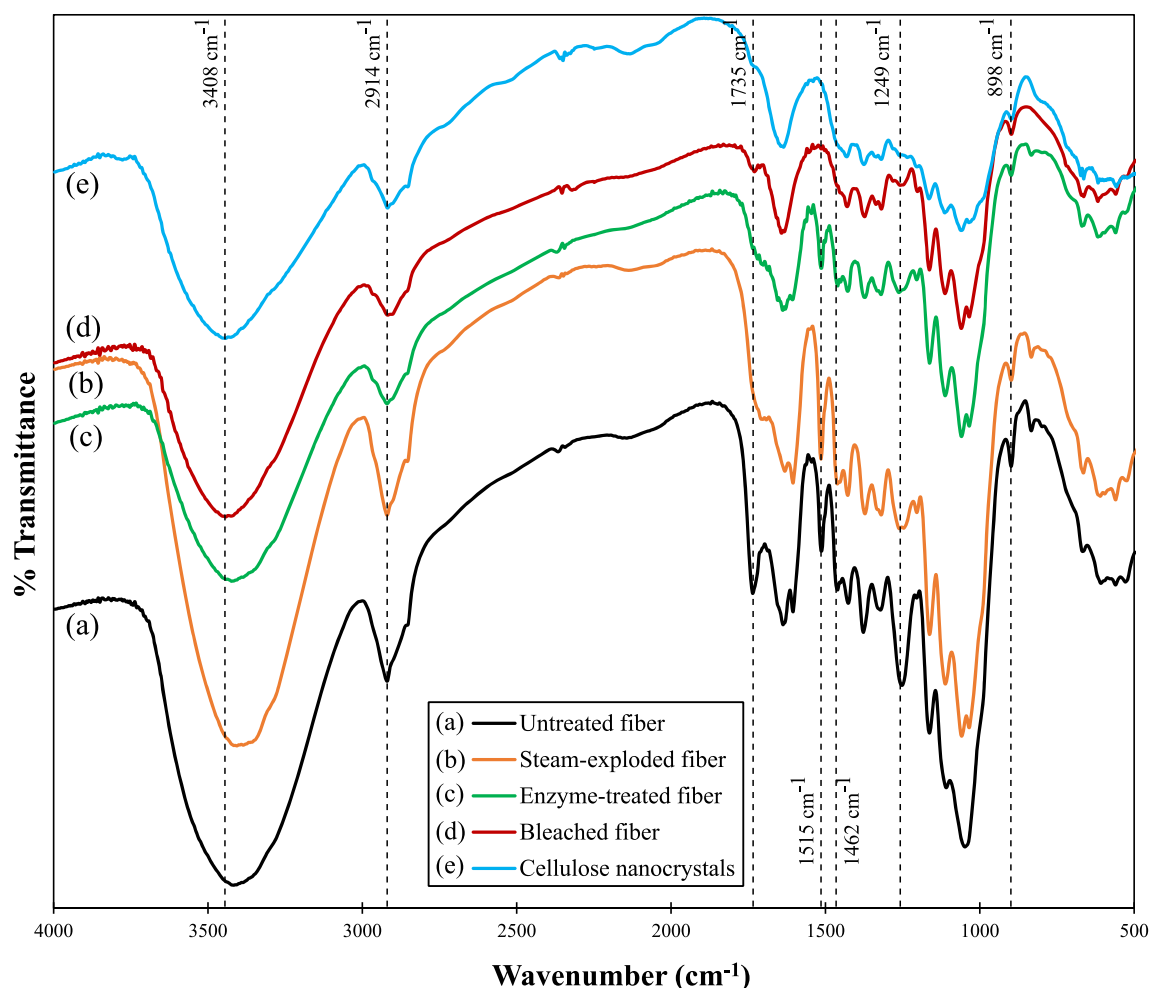


Fig. 5 FTIR spectra of untreated fiber (a), steam-exploded fiber (b), enzyme-treated fiber (c), bleached fiber (d) and cellulose nanocrystals (e)

stretching vibration (Mandal and Chakrabarty 2011). The 897 cm^{-1} band in all samples represented the glycosidic – C–H deformation, with a ring vibration contribution and – O–H bending which are known characteristics of β -glycosidic linkages between the anhydroglucose units in cellulose (Alemdar and Sain 2008).

The shape of the peak at 1730 cm^{-1} found in the spectrum of untreated fibers (Fig. 5a) was associated with the C–O stretching vibration for the acetyl and ester linkage in lignin or hemicellulose. Therefore, steam-exploded fiber and enzyme-treated fiber did not have this peak due to the removal of the hemicellulose and lignin to a certain extent (Saelee et al. 2016). The intensity of peak at 1249 cm^{-1} stood for the C–O out-of-plane stretching vibration of the aryl group in lignin and was substantially reduced in the spectrum of bleached fiber obtained after sodium chloride treatment (Troedec et al. 2008). Moreover, the spectral band at 1604, 1515 and 1460 cm^{-1} in the untreated fiber curve represented aromatic ring vibration and C–H deformation vibration of lignin. These peaks were also absent in the

bleached fiber spectrum (Rosa et al. 2010). These observations confirmed the successful elimination of lignin in the bleached fibers. There was no difference between the spectrum of nanocellulose and the bleached fibers.

X-Ray Diffraction

To evaluate the effect of each treatment on the resulting material based on the changing in crystallinity of the fibers, XRD was carried out. Figure 6 presents the XRD patterns of fibers obtained at different stages of purification. The crystallinity percentage of fibers at each stage is illustrated in Table 4.

From Fig. 6, all of the samples recorded similar diffraction patterns. However, the difference of slight intensity changes in the peaks was notable, as it represented minor changes in the level of order in the samples (Elanthikkal et al. 2010). The XRD pattern of each kind of fiber showed peaks around $2\theta = 16^\circ$ and 22.5° assigned to plane (110) and (200), which were believed to represent the

Fig. 6 XRD of untreated fiber (a), steam-exploded fiber (b), enzyme-treated fiber (c), bleached fiber (d) and cellulose nanocrystals (e)

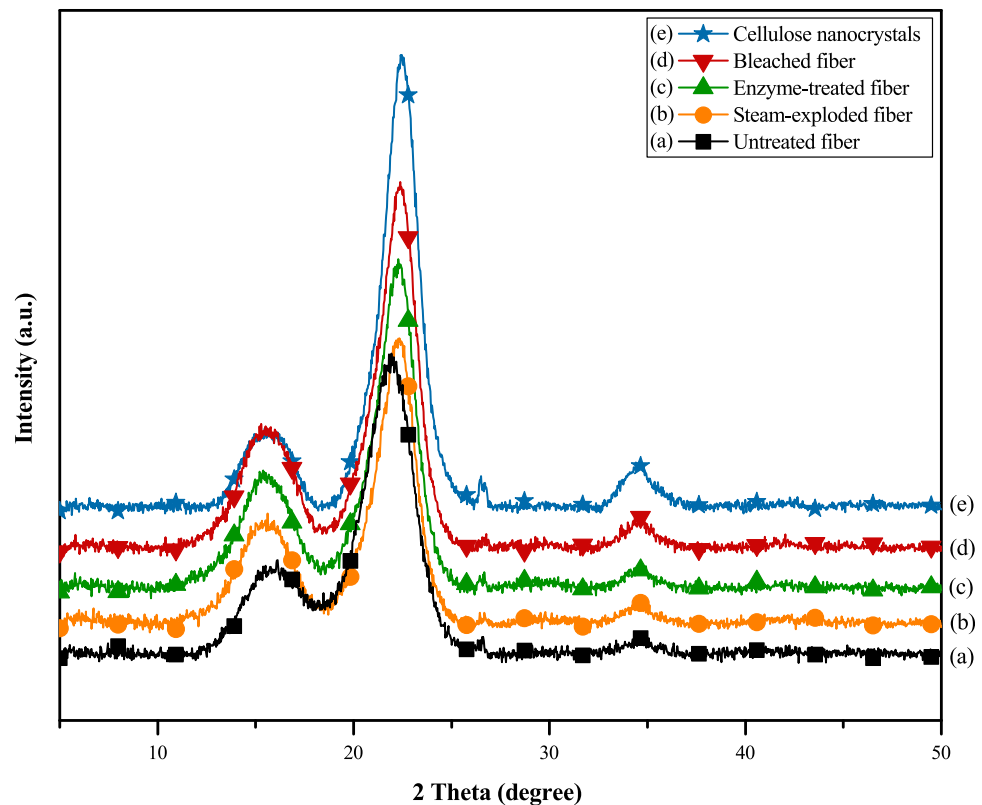


Table 4 Crystallinity Index (CrI) (mean value \pm standard deviation) of the fibers after different stages of treatment

Sample	Crystallinity Index (%CrI)
Untreated fiber	47.38 \pm 1.18
Steam-exploded fiber	49.36 \pm 0.81
Enzyme-treated fiber	51.23 \pm 0.98
Bleached fiber	56.06 \pm 1.01
Cellulose nanocrystals	68.54 \pm 1.30

polymorphs of cellulose I (Klemm et al. 2005). An increased trend toward crystallinity after each treatment stage confirmed the hemicellulose and lignin removal, with figures of 49.36 \pm 0.81% for steam-exploded fiber and 51.23 \pm 0.98% for enzyme-treated fiber. The bleached fiber recorded 56.06 \pm 1.01% of CrI, which was higher than for untreated fiber (47.38 \pm 1.18%) due to the elimination of noncellulosic components (Saelee et al. 2016). It is well documented that the cellulose structure includes a strong connection between the amorphous domain and the crystalline region by hydrogen bonding, which results in an ordered system with crystal-like properties. (Alemdar and Sain 2008). The effect of sulfuric acid in the crystallinity improvement of CNCs (68.54 \pm 1.30%) in comparison with bleached fiber is shown in Fig. 6e and could be explained by the CNCs structure being regarded as free

amorphous domains that were readily degraded during acid hydrolysis (Azizi Samir et al. 2004).

Thermal Analysis

Figure 7a, b shows the thermal properties resulting from the including thermogravimetry (TG) and derivative thermogravimetry (DTG) analysis of fibers. The TG graph indicates changes in weight during heating, and their derivatives show changes in the TG slope which may not be obvious from the TG curve. Table 5 displays the onset of thermal decomposition (T_{on}) indicating the beginning of degradation temperature and the temperature of maximum decomposition (T_{max}) referred to as the temperature of the maximum rate of degradation. Clearly, the initial mass losses starting at 75 °C for untreated, steam-exploded, enzyme-treated, bleached fibers and CNCs indicated the evaporation of loose, surface-bound moisture (H_2O). The intermolecular H-bonded water was evaporated at around 100 °C in all samples. The degradation of untreated fiber started at 280 °C, and the rate of degradation reached its peak at 357 °C (observed from the DTG curve) while that of bleached fibers occurred at 328 °C and achieved the maximum rate degradation at 351 °C. The degradation of CNCs occurred afterward at 250 °C, showing an additional small shoulder, and the rate of degradation was reached at 268 °C (also observed from the DTG curve). The untreated

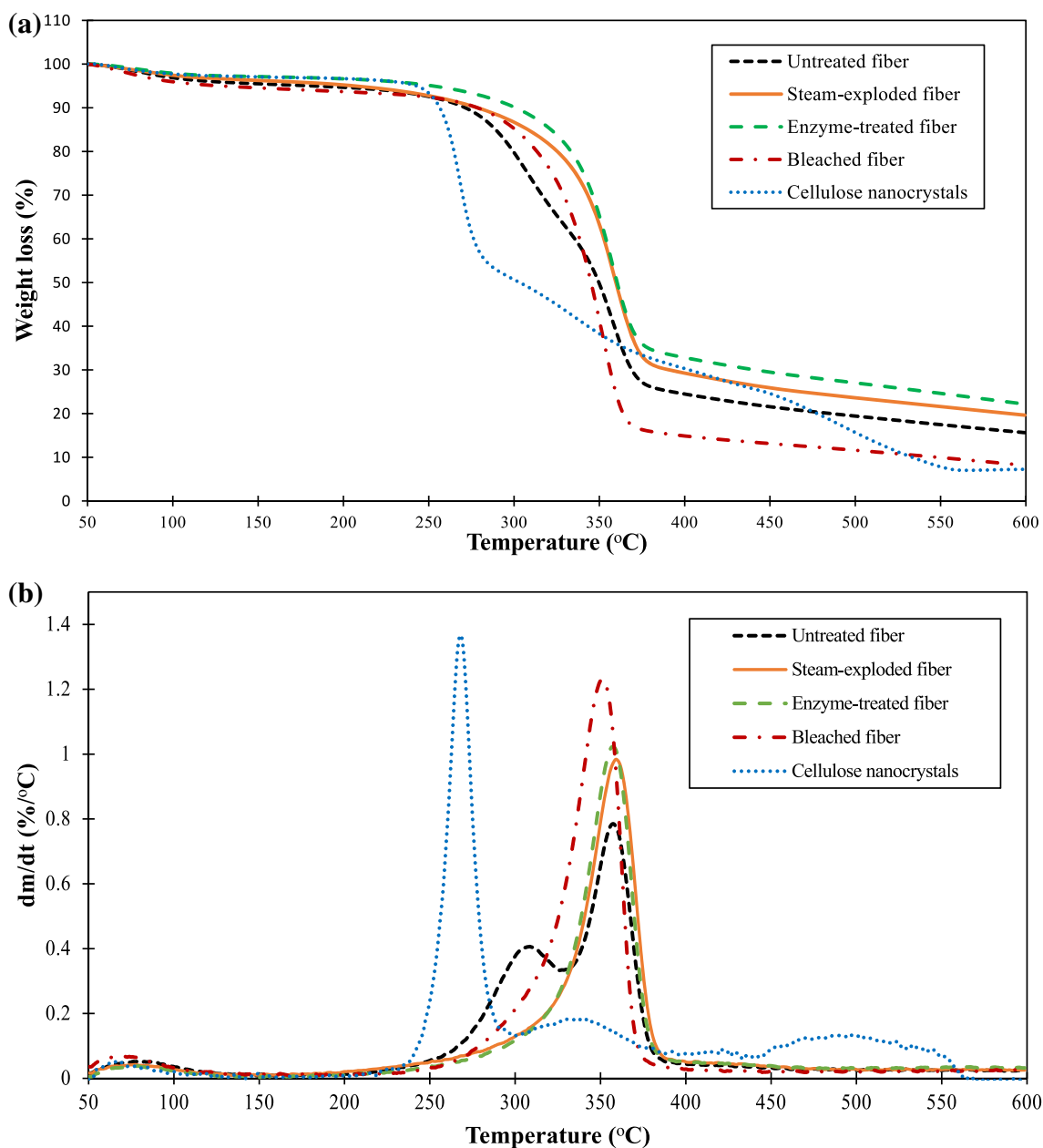


Fig. 7 TG (a) and DTG (b) curves of untreated fiber, steam-exploded fiber, enzyme-treated fiber, bleached fiber and cellulose nanocrystals

fiber illustrated a shoulder in its DTG curve at approximately 300 °C that resembled hemicellulose decomposition. In the curve of the steam-exploded fiber, the lack of this shoulder peak confirmed hemicellulose elimination. Moreover, the increase in T_{on} in steam-exploded fibers revealed the effect of the steam-explosion treatment on the removal of hemicellulose and partial lignin degradation. In the second stage, the removal of hemicellulose by xylanase treatment resulted in the improved thermal stability of the enzyme-treated fibers. A DTG analysis of the enzyme-treated fibers showed that T_{on} and T_{max} shifted to 332 °C (weight loss 6.2%) and 357 °C (weight loss 45.28%),

respectively. The same trend was observed in the enzyme-treated fiber and bleached fiber. The bleaching process was pyrolyzed at a slightly lower temperature of 328 °C (weight loss 10%) compared to that of xylanase-treated fiber and reached a T_{max} of 351 °C (weight loss 61%) due to diameter of bleached fibers reduction. The improvement in thermal stability could have been due to the noncellulosic components, which were considered low crystal structures, being liberated during the bleaching process.

With the CNCs, thermal degradation occurred in a lower temperature range starting at a T_{on} of 250 °C and extending to a T_{max} of 268 °C. Simultaneously, the CNCs were less

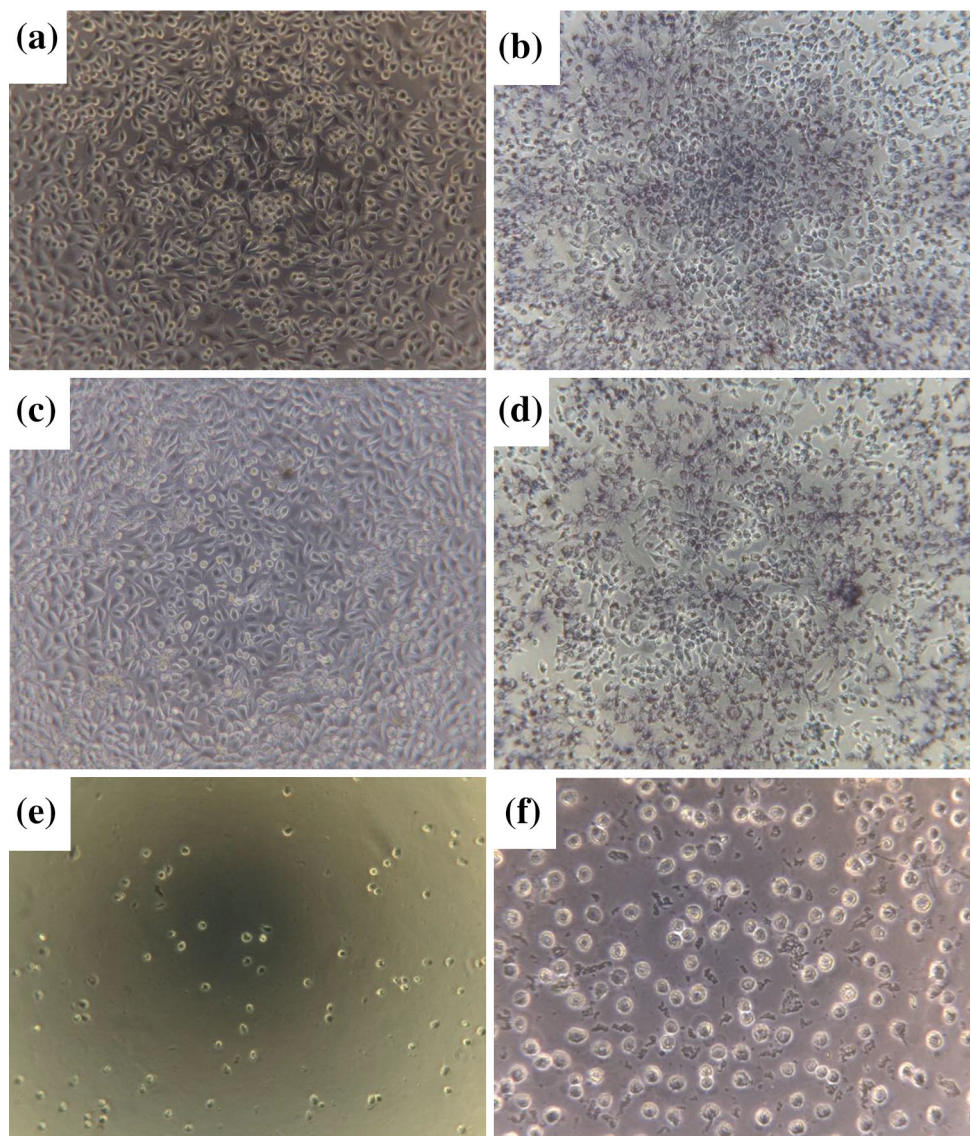
Table 5 Thermal properties of the fibers after different stages of treatment

Sample	T_{onset} (°C)	Mass loss (%)	T_{max} (°C)	Mass loss (%)	Residue at 600 °C (%)
Untreated fiber	280	07.00	357	58.30	15.63
Steam-exploded fiber	330	07.80	359	49.41	19.62
Enzyme-treated fiber	332	06.20	357	45.28	22.16
Bleached fiber	328	10.00	351	61.03	08.16
Cellulose nanocrystals	250	03.20	268	26.21	07.25

thermally stable than bleached fibers, as the DTG curve of the CNCs displays three stages of pyrolysis, mainly at 240–300, 300–380 and 450–550 °C, respectively (Wang et al. 2007). The T_{max} presented as the main peak in the DTG curve was at a much lower temperature than that of native cellulose (around 400 °C) (George et al. 2008)

perhaps because the acid-hydrolyzed cellulose was reduced to the size of nanometers and this increased the surface area and the number of free ends in the chain that were more accessible to degradation. Furthermore, the CNCs illustrated two humps or shoulders in close proximity on the DTG curve. The lower temperature degradation was

Fig. 8 Optical microscopy images ($\times 100$) of cultured L929 cells after one day of incubation **a** negative control, **c** CNCs, **e** positive control and after MTT assay of **b** negative control, **d** CNCs and **f** positive control



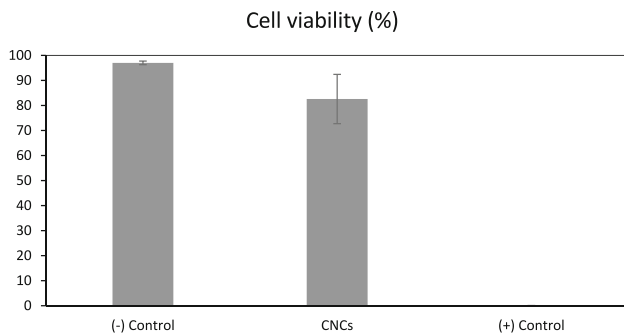


Fig. 9 Cell viability results (mean value) of CNCs, negative and positive control (*bars* represent standard deviation of the mean)

associated with the sulfated region of nanoparticles during pyrolysis while the other was due to degradation of the unsulfated part (Roman and Winter 2004).

Cytotoxicity

Cytotoxicity analysis of the CNCs used in this study was performed in accordance with ISO standard 10993-5:2009 (E) Annex C. In this study, the MTT assay was performed to evaluate the cell proliferation of the L929 cell line. The microscopic morphology of the L929 cell line that was observed following culture in positive (cytotoxic), negative (nontoxic) and CNCs extractive media is illustrated in Fig. 8. There was no difference in the L929 cell morphology after incubating for 24 h between the negative control and the media with the presence of CNCs. Figure 9 shows the cell viability results comparison of CNCs with the negative and positive controls. The viability threshold for the cytotoxicity analysis was 70%. The relative cell numbers cultured with the extraction medium including CNCs was significantly higher than that of the positive control plate, with figures of 83 and 0%, respectively. CNCs have been well recognized as nontoxic materials for cells showing more than 70% cell viability (Dong et al. 2012). This result suggested that the extract from CNCs produced no harmful effects to cell growth and thus, it can be concluded that CNCs are a material with no cytotoxic potential.

Conclusion

Cellulose nanocrystals (CNCs) were successfully obtained using acid hydrolysis from bleached fibers that could be purified by steam-explosion and enzyme-assisted pretreatment. The morphological properties indicated a needle-like shape of CNCs with an aspect ratio (L/d) of 20–25. The results from FTIR spectroscopy and XRD also confirmed noncellulose removal and an improvement in the

crystallinity percentage. However, the TGA curve illustrated a decline in the thermal persistence of nanoparticles due to the introduction of sulfate groups on their surfaces. Furthermore, MTT assay revealed the potential of CNCs for biomedical application, with a cell viability of 83%.

Acknowledgements The authors are grateful to the Thailand Research Fund (TRF) for financial support, the Department of Biotechnology, Faculty of Agro-Industry and Kasetsart University, Thailand for supplying facilities, the Scholarship Program for International Graduate Students 2014; and the National Center for Genetic Engineering and Biotechnology (BIOTEC), Thailand for providing xylanase enzyme.

Funding This study was funded by Thailand Research fund (Grant Number TRF5850012).

Compliance with Ethical Standards

Conflict of interest All authors of this research paper declare that that have no conflict of interest.

References

- Abraham, E., B. Deepa, L.A. Pothan, M. Jacob, S. Thomas, U. Cvelbar, and R. Anandjiwala. 2011. Extraction of nanocellulose fibrils from lignocellulosic fibres: A novel approach. *Carbohydrate Polymers* 86 (4): 1468–1475. doi:10.1016/j.carbpol.2011.06.034.
- Alemdar, Ayse, and Mohini Sain. 2008. Biocomposites from wheat straw nanofibers: Morphology, thermal and mechanical properties. *Composites Science and Technology* 68 (2): 557–565. doi:10.1016/j.compscitech.2007.05.044.
- Bhattacharya, Deepanjan, Louis T. Germinario, and William T. Winter. 2008. Isolation, preparation and characterization of cellulose microfibrils obtained from bagasse. *Carbohydrate Polymers* 73 (3): 371–377. doi:10.1016/j.carbpol.2007.12.005.
- Brinchi, L., F. Cotana, E. Fortunati, and J.M. Kenny. 2013. Production of nanocrystalline cellulose from lignocellulosic biomass: Technology and applications. *Carbohydrate Polymers* 94 (1): 154–169. doi:10.1016/j.carbpol.2013.01.033.
- Chen, Wenshuai, Yu. Haipeng, Yixing Liu, Peng Chen, Mingxin Zhang, and Yunfei Hai. 2011. Individualization of cellulose nanofibers from wood using high-intensity ultrasonication combined with chemical pretreatments. *Carbohydrate Polymers* 83 (4): 1804–1811. doi:10.1016/j.carbpol.2010.10.040.
- Dong, S., A.A. Hirani, K.R. Colacino, Y.W. Lee, and M. Roman. 2012. Cytotoxicity and cellular uptake of cellulose nanocrystals. *Nano Life* 02 (03): 124106. doi:10.1142/S1793984412410061.
- Dri, Fernando L., Louis G. Hector, Robert J. Moon, and Pablo D. Zavattieri. 2013. Anisotropy of the elastic properties of crystalline cellulose I β from first principles density functional theory with Van Der Waals interactions. *Cellulose* 20 (6): 2703–2718. doi:10.1007/s10570-013-0071-8.
- Eichhorn, S.J., A. Dufresne, M. Aranguren, N.E. Marcovich, J.R. Capadona, S.J. Rowan, C. Weder, et al. 2010. Review: Current international research into cellulose nanofibres and nanocomposites. *Journal of Materials Science* 45 (1): 1–33. doi:10.1007/s10853-009-3874-0.
- Elanthikkal, Silviya, Unnikrishnan Gopalakrishnanpanicker, Soney Varghese, and James T. Guthrie. 2010. Cellulose microfibrils

- produced from banana plant wastes: Isolation and characterization. *Carbohydrate Polymers* 80 (3): 852–859. doi: [10.1016/j.carbpol.2009.12.043](https://doi.org/10.1016/j.carbpol.2009.12.043).
- George, Johnsy, V.A. Sajeevkumar, R. Kumar, K.V. Ramana, S.N. Sabapathy, and A.S. Bawa. 2008. Enhancement of thermal stability associated with the chemical treatment of bacterial (*Gluconacetobacter xylinus*) cellulose. *Journal of Applied Polymer Science* 108 (3): 1845–1851. doi: [10.1002/app.27802](https://doi.org/10.1002/app.27802).
- Gilbert, R.D., and J.F. Kadla. 2000. Polysaccharides-cellulose. In *Biopolymers from renewable resources. Macromolecular systems—material approach*, ed. D. Kaplan, 47–90. Berlin, Heidelberg: Springer.
- Kargarzadeh, Hanieh, Ishak Ahmad, Ibrahim Abdullah, Alain Dufresne, Siti Yasmine Zainudin, and Rasha M. Sheltami. 2012. Effects of hydrolysis conditions on the morphology, crystallinity, and thermal stability of cellulose nanocrystals extracted from kenaf bast fibers. *Cellulose* 19 (3): 855–866. doi: [10.1007/s10570-012-9684-6](https://doi.org/10.1007/s10570-012-9684-6).
- Khalil, H.P.S.A., H. Ismail, H.D. Rozman, and M.N. Ahmad. 2001. The effect of acetylation on interfacial shear strength between plant fibres and various matrices. *European Polymer Journal* 37 (5): 1037–1045. doi: [10.1016/s0014-3057\(00\)00199-3](https://doi.org/10.1016/s0014-3057(00)00199-3).
- Kim, D.H., and Y.S. Song. 2015. Anisotropic optical film embedded with cellulose nanowhisker. *Carbohydrate Polymers* 130: 448–454. doi: [10.1016/j.carbpol.2015.05.033](https://doi.org/10.1016/j.carbpol.2015.05.033).
- Kirdponpattara, S., A. Khamkeaw, N. Sanchavanakit, P. Pavasant, and M. Phisalaphong. 2015. Structural modification and characterization of bacterial cellulose-alginate composite scaffolds for tissue engineering. *Carbohydrate Polymers* 132: 146–155. doi: [10.1016/j.carbpol.2015.06.059](https://doi.org/10.1016/j.carbpol.2015.06.059).
- Klemm, Dieter, Brigitte Heublein, Hans-Peter Fink, and Andreas Bohn. 2005. Cellulose: Fascinating biopolymer and sustainable raw material. *Angewandte Chemie International Edition* 44 (22): 3358–3393. doi: [10.1002/anie.200460587](https://doi.org/10.1002/anie.200460587).
- Kumar, Anuj, Yuvraj Singh Negi, Nishi Kant Bhardwaj, and Veena Choudhary. 2012. Synthesis and characterization of methylcellulose/PVA based porous composite. *Carbohydrate Polymers* 88 (4): 1364–1372. doi: [10.1016/j.carbpol.2012.02.019](https://doi.org/10.1016/j.carbpol.2012.02.019).
- Kumar, Anuj, Yuvraj Singh Negi, Veena Choudhary, and Nishi Kant Bhardwaj. 2014. Microstructural and mechanical properties of porous biocomposite scaffolds based on polyvinyl alcohol. *Nano-Hydroxyapatite and Cellulose Nanocrystals. Cellulose* 21 (5): 3409–3426. doi: [10.1007/s10570-014-0339-7](https://doi.org/10.1007/s10570-014-0339-7).
- Kuzmenko, Volodymyr, Theodoros Kalogeropoulos, Johannes Thunberg, Sara Johannesson, Daniel Hägg, Peter Enoksson, and Paul Gatenholm. 2016. Enhanced growth of neural networks on conductive cellulose-derived nanofibrous scaffolds. *Materials Science and Engineering, C: Materials for Biological Applications* 58: 14–23. doi: [10.1016/j.msec.2015.08.012](https://doi.org/10.1016/j.msec.2015.08.012).
- Le Troedec, Marianne, David Sedan, Claire Peyratout, Jean Pierre Bonnet, Agnès Smith, René Guinebretiere, Vincent Gloaguen, and Pierre Krausz. 2008. Influence of various chemical treatments on the composition and structure of hemp fibres. *Composites Part A Applied Science and Manufacturing* 39 (3): 514–522. doi: [10.1016/j.compositesa.2007.12.001](https://doi.org/10.1016/j.compositesa.2007.12.001).
- Li, M., L.J. Wang, D. Li, Y.L. Cheng, and B. Adhikari. 2014. Preparation and characterization of cellulose nanofibers from depectinated sugar beet pulp. *Carbohydrate Polymers* 102: 136–143. doi: [10.1016/j.carbpol.2013.11.021](https://doi.org/10.1016/j.carbpol.2013.11.021).
- Male, Keith B., Alfred C.W. Leung, Johnny Montes, Amine Kamen, and John H.T. Luong. 2012. Probing inhibitory effects of nanocrystalline cellulose: Inhibition versus surface charge. *Nanoscale* 4 (4): 1373–1379. doi: [10.1039/C2NR11886F](https://doi.org/10.1039/C2NR11886F).
- Mandal, A., and D. Chakrabarty. 2011. Isolation of nanocellulose from waste sugarcane bagasse (scb) and its characterization. *Carbohydrate Polymers* 86 (3): 1291–1299. doi: [10.1016/j.carbpol.2011.06.030](https://doi.org/10.1016/j.carbpol.2011.06.030).
- Mariano, Marcos, Nadia El Kissi, and Alain Dufresne. 2014. Cellulose nanocrystals and related nanocomposites: Review of some properties and challenges. *Journal of Polymer Science Part B: Polymer Physics* 52 (12): 791–806. doi: [10.1002/polb.23490](https://doi.org/10.1002/polb.23490).
- Marzieh, Shafiei, Kumar Rajeev, and Keikhosro Karimi. 2015. Pretreatment of lignocellulosic biomass. In *Lignocellulose-based bioproducts*, vol. 1, ed. K. Karimi, 85–154. Switzerland: Springer International Publishing.
- Petersson, L., and K. Oksman. 2006. Biopolymer based nanocomposites: Comparing layered silicates and microcrystalline cellulose as nanoreinforcement. *Composites Science and Technology* 66 (13): 2187–2196. doi: [10.1016/j.compscitech.2005.12.010](https://doi.org/10.1016/j.compscitech.2005.12.010).
- Ranby, B.G. 1949. Aqueous colloidal solutions of cellulose micelles. *Acta Chemica Scandinavica* 3: 649–650.
- Rhim, J.W., Y. Wu, C.L. Weller, and M. Schnepf. 1999. Physical characteristics of a composite film of soy protein isolate and propyleneglycol alginate. *Journal of Food Science* 64 (1): 149–152. doi: [10.1111/j.1365-2621.1999.tb09880.x](https://doi.org/10.1111/j.1365-2621.1999.tb09880.x).
- Roman, Maren, and William T. Winter. 2004. Effect of sulfate groups from sulfuric acid hydrolysis on the thermal degradation behavior of bacterial cellulose. *Biomacromolecules* 5 (5): 1671–1677. doi: [10.1021/bm034519+](https://doi.org/10.1021/bm034519+).
- Roncero, M. Blanca, Antonio L. Torres, Jos F. Colom, and Teresa Vidal. 2003. Effect of xylanase on ozone bleaching kinetics and properties of *Eucalyptus* kraft pulp. *Journal of Chemical Technology and Biotechnology* 78 (10): 1023–1031. doi: [10.1002/jctb.893](https://doi.org/10.1002/jctb.893).
- Rosa, M.F., E.S. Medeiros, J.A. Malmonge, K.S. Gregorski, D.F. Wood, L.H.C. Mattoso, G. Glenn, W.J. Orts, and S.H. Imam. 2010. Cellulose nanowhiskers from coconut husk fibers: Effect of preparation conditions on their thermal and morphological behavior. *Carbohydrate Polymers* 81 (1): 83–92. doi: [10.1016/j.carbpol.2010.01.059](https://doi.org/10.1016/j.carbpol.2010.01.059).
- Saelee, Kullasatri, Naiyasit Yingkamhaeng, Thidarat Nimchua, and Prakrit Sukyai. 2016. An environmentally friendly xylanase-assisted pretreatment for cellulose nanofibrils isolation from sugarcane bagasse by high-pressure homogenization. *Industrial Crops and Products* 82: 149–160. doi: [10.1016/j.indcrop.2015.11.064](https://doi.org/10.1016/j.indcrop.2015.11.064).
- Samir, Azizi, My Ahmed Said, Fannie Alloin, Jean-Yves Sanchez, and Alain Dufresne. 2004. Cellulose nanocrystals reinforced poly(oxyethylene). *Polymer* 45 (12): 4149–4157. doi: [10.1016/j.polymer.2004.03.094](https://doi.org/10.1016/j.polymer.2004.03.094).
- Segal, L., J.J. Creely, A.E. Jr Martin, and C.M. Conrad. 1962. An empirical method for estimating the degree of crystallinity of native cellulose using the x-ray diffractometer. *Textile Research Journal* 29: 786–794.
- Šturcová, Adriana, Geoffrey R. Davies, and Stephen J. Eichhorn. 2005. Elastic modulus and stress-transfer properties of tunicate cellulose whiskers. *Biomacromolecules* 6 (2): 1055–1061. doi: [10.1021/bm049291k](https://doi.org/10.1021/bm049291k).
- Sun, Ye, and Jiayang Cheng. 2002. Hydrolysis of lignocellulosic materials for ethanol production: A review. *Bioresource Technology* 83 (1): 1–11.
- Sun, J.X., X.F. Sun, R.C. Sun, and Y.Q. Su. 2004. Fractional extraction and structural characterization of sugarcane bagasse hemicelluloses. *Carbohydrate Polymers* 56 (2): 195–204. doi: [10.1016/j.carbpol.2004.02.002](https://doi.org/10.1016/j.carbpol.2004.02.002).
- Sun, X.F., F. Xu, R.C. Sun, P. Fowler, and M.S. Baird. 2005. Characteristics of degraded cellulose obtained from steam-exploded wheat straw. *Carbohydrate Research* 340 (1): 97–106. doi: [10.1016/j.carres.2004.10.022](https://doi.org/10.1016/j.carres.2004.10.022).
- Teixeira, Eliangela de Morais, Ana Carolina Corrêa, Alexandra Manzoli, Fabio de Lima Leite, Cauê Ribeiro de Oliveira, and Luiz Henrique Capparelli Mattoso. 2010. Cellulose nanofibers

- from white and naturally colored cotton fibers. *Cellulose* 17 (3): 595–606. doi:[10.1007/s10570-010-9403-0](https://doi.org/10.1007/s10570-010-9403-0).
- Teixeira, Eliangela, Thalita de Morais, Jessika Bondancia, Kelcilene Bruna Ricardo Teodoro, Ana Carolina Corrêa, José Manoel Marconcini, and Luiz Henrique Caparelli Mattoso. 2011. Sugarcane bagasse whiskers: Extraction and characterizations. *Industrial Crops and Products* 33 (1): 63–66. doi:[10.1016/j.indcrop.2010.08.009](https://doi.org/10.1016/j.indcrop.2010.08.009).
- Wang, Neng, Enyong Ding, and Rongshi Cheng. 2007. Thermal degradation behaviors of spherical cellulose nanocrystals with sulfate groups. *Polymer* 48 (12): 3486–3493. doi:[10.1016/j.polymer.2007.03.062](https://doi.org/10.1016/j.polymer.2007.03.062).
- Wang, Wei-Ming, Zai-Sheng Cai, Yu. Jian-Yong, and Zhao-Peng Xia. 2010. Changes in composition, structure, and properties of jute fibers after chemical treatments. *Fibers and Polymers* 10 (6): 776–780. doi:[10.1007/s12221-009-0776-3](https://doi.org/10.1007/s12221-009-0776-3).
- Wu, Xiawa, Robert J. Moon, and Ashlie Martini. 2012. Crystalline cellulose elastic modulus predicted by atomistic models of uniform deformation and nanoscale indentation. *Cellulose* 20 (1): 43–55. doi:[10.1007/s10570-012-9823-0](https://doi.org/10.1007/s10570-012-9823-0).
- Zhang, L.H., D. Li, L.J. Wang, T.P. Wang, L. Zhang, X.D. Chen, and Z.H. Mao. 2008. Effect of steam explosion on biodegradation of lignin in wheat straw. *Bioresource Technology* 99 (17): 8512–8515. doi:[10.1016/j.biortech.2008.03.028](https://doi.org/10.1016/j.biortech.2008.03.028).
- Zheng, Yi, Jia Zhao, Xu Fuqing, and Yebo Li. 2014. Pretreatment of lignocellulosic biomass for enhanced biogas production. *Progress in Energy and Combustion Science* 42: 35–53. doi:[10.1016/j.peccs.2014.01.001](https://doi.org/10.1016/j.peccs.2014.01.001).
- Zhou, Y.M. 2012. Effect of nanocellulose isolation techniques on the formation of reinforced poly(vinyl alcohol) nanocomposite films. *Express Polymer Letters* 6 (10): 794–804. doi:[10.3144/expresspolymlett.2012.85](https://doi.org/10.3144/expresspolymlett.2012.85).
- Zhou, Chengjun, Qingfeng Shi, Weihong Guo, Lekeith Terrell, Ammar T. Qureshi, Daniel J. Hayes, and Wu Qinglin. 2013. Electrospun bio-nanocomposite scaffolds for bone tissue engineering by cellulose nanocrystals reinforcing maleic anhydride grafted PLA. *ACS Applied Materials and Interfaces* 5 (9): 3847–3854. doi:[10.1021/am4005072](https://doi.org/10.1021/am4005072).
- Zuluaga, Robin, Jean Luc Putaux, Javier Cruz, Juan Vélez, Iñaki Mondragon, and Piedad Gañán. 2009. Cellulose microfibrils from banana rachis: Effect of alkaline treatments on structural and morphological features. *Carbohydrate Polymers* 76 (1): 51–59. doi:[10.1016/j.carbpol.2008.09.024](https://doi.org/10.1016/j.carbpol.2008.09.024).